



Research paper

Low pressure experiments in piston cylinder apparatus: Calibration of newly designed 25 mm furnace assemblies to $P = 150$ MPa

Matteo Masotta ^{a,*}, Carmela Freda ^b, Tracy A. Paul ^c, Gordon M. Moore ^d, Mario Gaeta ^{a,b}, Piergiorgio Scarlato ^b, Valentin R. Troll ^{b,e}

^a Dipartimento di Scienze della Terra, Sapienza – Università di Roma, P.le Aldo Moro, 5, 00185, Rome, Italy

^b Istituto Nazionale di Geofisica e Vulcanologia, Via di Vigna Murata, 605, 00143, Rome, Italy

^c Depths of the Earth Co., 6314 East Morning Vista Lane, Cave Creek, Arizona 85331-6701, USA

^d Department of Chemistry and Biochemistry, Arizona State University, Tempe, Arizona 85287-1604, USA

^e Department of Earth Sciences, CEMPEG, Uppsala University, Villavägen 16, 752 36 Uppsala, Sweden

ARTICLE INFO

Article history:

Received 6 October 2011

Received in revised form 28 February 2012

Accepted 17 April 2012

Available online 25 April 2012

Editor: D.B. Dingwell

Keywords:

Piston cylinder

Pressure calibration

NaCl melting

H₂O solubility

Low pressure

ABSTRACT

We present new pressure calibration experiments demonstrating that the piston cylinder apparatus is suitable for experiments at pressure as low as 150 MPa. Two newly designed 25 mm furnace assembly have been developed and calibrated using two different calibration methods: the NaCl melting curve and the solubility of H₂O in albitic and rhyolitic melts. The NaCl calibration experiments performed in the pressure range 150–500 MPa yield the pressure correction that has to be applied to the nominal pressure in order to have the equivalent (real) pressure on the sample. This correction varies as a function of the experimental pressure as follows:

$$P_{\text{correction}}(\text{MPa}) = -0.115 \times P_{\text{nominal}}(\text{MPa}) + 78.23$$

The H₂O solubility experiments in albitic and rhyolitic melts confirm the corrections determined using the NaCl calibration method. Moreover, because these experiments are performed at temperatures higher than those used for NaCl calibration, they demonstrate that the pressure correction is not affected by temperature in the range 800–1000 °C. The accuracy of the pressure estimate associated with the calibration methods is ± 25 MPa.

The major advantage of using the new assemblies is that low pressure experiments, which require rapid heating and quenching rates (e.g. volcanic and hydrothermal systems), can be performed with the same ease and precision as standard high pressure experiments for which piston cylinder is routinely used.

© 2012 Elsevier B.V. All rights reserved.

1. Introduction

The piston cylinder apparatus (Boyd and England, 1960) is one of the most versatile instruments operating in experimental petrology laboratories because it provides a safe, inexpensive, and easy-to-use technique for accessing high pressure and high temperature conditions. The operating pressure of the piston cylinder usually ranges between 0.5 and 5 GPa (Johannes et al., 1971; Holloway and Wood, 1988; Nelson and Montana, 1992), which allows scientists to investigate materials and processes under deep crustal to upper mantle conditions. Incomplete compaction of the furnace assembly and thermocouple failure are typical problems in experiments performed at pressures lower than 0.5 GPa (Moore et al., 2008). Due to this operative limit, internally heated pressure vessels and cold seal pressure vessels are commonly

preferred for low pressure experiments (i.e. ≤ 0.5 GPa). However, unlike gas media pressure vessels, the piston cylinder apparatus offers faster heating and cooling rates, lower operating effort and maintenance, and increased safety, thereby making the device advantageous for geochemical studies, including phase equilibria, volatile solubility, and chemical diffusion in volcanic systems. For these reasons, experimentalists have invested considerable time and effort to calibrate the piston cylinder for pressures lower than 0.5 GPa. Pressure calibration implies correction of the nominal pressure (i.e. force applied to the piston) that generally differs from the real pressure inside the sample, due to the internal friction in the assembly. Pressure corrections vary according with operative conditions (temperature and pressure) and assembly components. Baker (2004) demonstrated that the piston cylinder can be calibrated and operated reliably down to 400 MPa. More recently, experiments were successfully performed at a yet lower limit of 300 MPa (Moore et al., 2008; Masotta et al., 2012). In this work, two new designs of crushable MgO–Glass–NaCl furnace assemblies are used to calibrate a non-end loaded piston cylinder apparatus

* Corresponding author. Tel.: +39 06 51860502; fax: +39 06 51860507.
E-mail address: matteo.masotta@uniroma1.it (M. Masotta).

down to 150 MPa. Calibration methods used are the NaCl melting curve and the solubility of H₂O in albitic and rhyolitic melts.

2. Experimental methods and analytical techniques

Experiments were carried out using non-end loaded piston cylinder apparatus (QUICKpress design by Depths of the Earth Co.) at the Department of Chemistry and Biochemistry (Arizona State University, Tempe, AZ, US) and at the HP-HT Laboratory of Experimental Volcanology and Geophysics (Istituto Nazionale di Geofisica e Vulcanologia, Rome, Italy). Calibration experiments performed in the pressure range 300–500 MPa used a standard 19 mm assembly, whereas experiments in the pressure range 150–300 MPa used two newly designed 25 mm assemblies (see below). In each run, the assembly was cold pressurized to a nominal pressure 10% higher than that desired for the experiment and held for few minutes. Pressure was then decreased to the desired pressure and maintained constant for the duration of the experiment and during the quench. The heating was done in manual mode in order to avoid overshooting and to constrain the temperature oscillations around the set point to within 2 °C. Temperature was measured using either factory calibrated C-type (W₉₅Re₅–W₇₄Re₂₆) or K-type (chromel–alumel) thermocouples, both having a ± 5 °C uncertainty (Holtz et al., 2001). The oxygen fugacity in the standard 19 mm assembly is NNO + 2 (Masotta et al., 2012), in agreement with that calculated by Freda et al. (2008) using similar 19 mm assemblies (NaCl–crushable alumina–borosilicate glass). Because the 19–25 and 25 mm assemblies are comprised by the same materials as the standard 19 mm, we expect comparable oxygen fugacity values.

Field Emission Scanning Electron Microscope (FE-SEM) images and electron microprobe analyses (EMPA) of experimental products were obtained at the HP-HT Laboratory of Experimental Volcanology and Geophysics with a JEOL FE-SEM 6500F equipped with an energy dispersive microanalysis system and a JEOL-JXA8200 EDS-WDS combined electron microprobe, respectively. The electron microprobe is

equipped with five wavelength-dispersive spectrometers. Chemical analyses were performed using 15 kV accelerating voltage and 10 nA beam current and a defocused electron beam of 7 μ m and a counting time of 5 s on background and 15 s on peak. The following standards were used for analyses of rhyolitic glasses: orthoclase (Si, Al, and K), rutile (Ti), andradite (Fe), forsterite (Mg), spessartine (Mn), barite (Ba), jadeite (Na) and apatite (P). For analyses of the albitic glasses we used: albite (Si, Al, and Na) and orthoclase (K). Sodium and potassium were analyzed before any other element to reduce possible volatilization effects.

2.1. The 25 mm furnace assemblies

The low pressure (150–300 MPa) calibration experiments presented in this study (Table 1) were performed using two newly designed furnace assemblies. Both of these assemblies fit in a 25 mm pressure plate and are comprised of crushable MgO–borosilicate glass–NaCl components (Fig. 1). Differences between the two assemblies are the diameter of the graphite furnace, the thickness of the borosilicate insulator, and the NaCl cell. The first assembly, hereafter called 19–25 mm assembly, comprises an 11.0 mm outer diameter (OD) graphite furnace (as in the standard 19 mm assembly) and thick borosilicate glass insulator and NaCl cell. The second assembly, hereafter called 25 mm assembly, comprises an 18.2 mm OD graphite furnace and thin borosilicate glass insulator and NaCl cell. The larger diameter of the graphite furnace in the 25 mm assembly requires substantial current when operating at high temperature (i.e. $T \geq 1100$ °C) and, therefore, is best suited for experiments below 1100 °C. The 25 mm assembly is also characterised by a slightly lower quench rate (ca. 50 °C/s in the first 5 s) than the 19–25 mm assembly (ca. 100 °C/s in the first 5 s). The primary advantage of using the 25 mm assembly is the large volume that it can accommodate, either up to four small capsules (3 mm OD) or one large, single capsule (up to 10 mm OD), whereas only one capsule (up to 5 mm OD) can be accommodated in the 19–25 mm assembly.

Table 1
List of calibration experiments.

Sample	Assembly (mm)	Calibration method	T (°C)	Nominal pressure ^a (MPa)	Real pressure ^b (MPa)	Run duration (h)	Note
QP34-4	19	NaCl	911	505	483	0.3	Molten NaCl
QP34-6	19	NaCl	906	520	500	0.3	Solid NaCl
QP34-12	19	NaCl	862	337	293	0.3	Solid NaCl
QP34-13	19	NaCl	875	337	293	0.3	Molten NaCl
QP1-12	19–25	NaCl	862	336	292	0.3	Solid NaCl
QP1-13	19–25	NaCl	875	336	292	0.3	Molten NaCl
MIA-2	19–25	NaCl	853	200	138	0.3	Molten NaCl
MIA-3	19–25	NaCl	842	203	142	0.3	Molten NaCl
MIA-4	19–25	NaCl	842	224	166	0.3	Molten NaCl
MIA-5	19–25	NaCl	840	241	185	0.3	Solid NaCl
QP1-17	19–25	NaCl	834	221	162	0.3	Solid NaCl
QP1-18	19–25	NaCl	834	190	127	0.3	Molten NaCl
QP1-1	25	NaCl	840	259	205	0.3	Solid NaCl
QP1-2	25	NaCl	845	259	205	0.3	Solid NaCl
QP1-3	25	NaCl	848	259	205	0.3	Molten NaCl
QP1-4	25	NaCl	840	250	195	0.3	Solid NaCl
QP1-5	25	NaCl	848	241	185	0.3	Molten NaCl
QP1-19	25	NaCl	834	224	166	0.3	Solid NaCl
QP1-20	25	NaCl	834	210	150	0.3	Solid NaCl
QP1-21	25	NaCl	834	198	136	0.3	Molten NaCl
AB-1 ^c	25	H ₂ O + Ab	900	259	205	2	Hydrous
AB-3 ^c	25	H ₂ O + Ab	900	259	205	2	H ₂ O-sat
RIO-C6	25	H ₂ O + Rhy	975	210	150	24	H ₂ O-sat
RIO-C7 ^d	25	H ₂ O + Rhy	975	207	146	24	H ₂ O-sat
RIO-2 ^d	25	H ₂ O + Rhy	975	207	146	24	Hydrous

^a Nominal pressure, calculated from the nominal oil pressure using a multiplier based on the ratio of radii of the ram and piston (44.44 and 25.00 for the 19 mm and the 25 mm pressure plates, respectively).

^b Real pressure (i.e. sample pressure), calculated from Eq. (2).

^c Capsules run in tandem.

^d Capsules run in tandem.

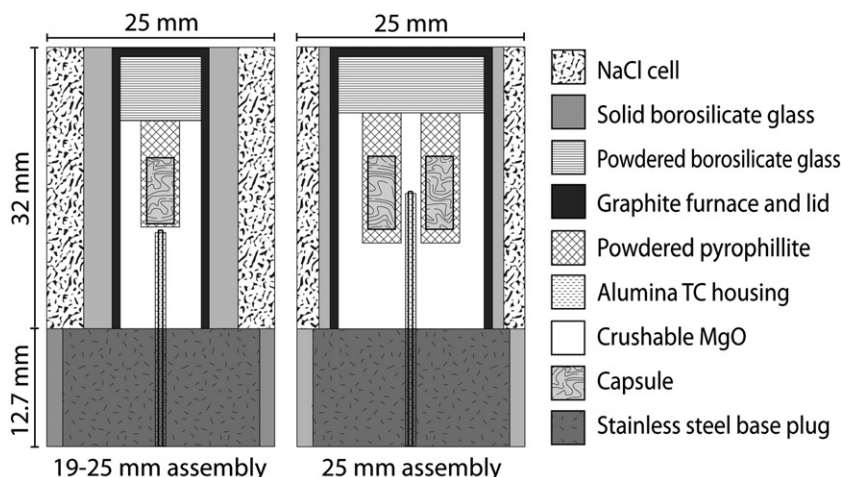


Fig. 1. Schematic cross sections of 19–25 mm and 25 mm furnace assemblies.

Despite these differences, the assemblies are similar and can be prepared following a similar protocol. In both designs, room for samples and thermocouple is created within the crushable MgO, according to the required geometry. In the 19–25 mm assembly the thermocouple is positioned below the sample, whereas in the 25 mm, the thermocouple connection is positioned at the half-length of the furnace, thus exploiting the whole hot spot zone (Fig. 1). To ensure easy extraction and cleaning of capsules after the experiment, the capsules are surrounded by either borosilicate glass powder or pyrophyllite powder. The use of pyrophyllite powder as soft supporting medium has the further advantage of inhibiting water loss from noble metal capsules (Freda et al., 2001). The crushable MgO-sample holder is inserted in the graphite furnace, a 5 mm thick layer of powdered borosilicate glass is used to fill the space up to the top of the furnace, and the graphite lid is positioned on top. Following the procedure of Moore et al. (2008), the four-bore alumina thermocouple housing is impregnated under vacuum using alumina cement (i.e. water and fine crushed alumina). This procedure is crucial because the impregnation inhibits the flow of soft material from the assembly into the thermocouple bore, thus preventing the failure of thermocouple when operating at low pressure. Then, thermocouple is inserted from the bottom of the assembly through the metal base plug, over which the sample holder and graphite furnace are seated. The insulating borosilicate glass sleeve and the NaCl salt cell are placed around the furnace and the complete assembly is seated on the metal base plug. The final height of the assembly is 44.7 mm (Fig. 1).

3. Results and discussion

3.1. NaCl calibration

The NaCl melting method (Bohlen, 1984) has been used to calibrate pressure at 500, 300, 200, and 150 MPa and the solubility of H₂O in albitic and rhyolitic melts has been used to confirm the results at 200 and 150 MPa.

For the NaCl melting method, noble metal capsules (AuPd or Pt, 3 mm diameter) were filled with reagent-grade NaCl and a Pt sphere (ca. 0.5 mm diameter) was positioned at the top. The capsules were then dried at 110 °C for 1 h before welded closed. Calibration charges were run at the NaCl melting temperatures in the pressure range 150–500 MPa and held at the experimental conditions for 20 min (NaCl melting curve from Siewert et al., 1998). After each run the capsule was sanded longitudinally and the position of the Pt sphere was checked by binocular. The falling of the sphere at the bottom of the capsule indicates the melting of the salt. The calibration experiments

performed at different T–P conditions constrained the position of the NaCl melting curve at pressures higher than those predicted by Siewert et al. (1998), thus indicating a mismatch between the real pressure (on the sample) and the nominal pressure (force applied to the piston). This difference implies a pressure correction which for both, 19–25 mm and 25 mm assemblies, decreases at increasing experimental pressure. In particular, the pressure corrections are +60 MPa at 150 MPa, +55 MPa at 200 MPa, and +45 MPa at 300 MPa. For example, in order to obtain a real pressure of 300 MPa, the nominal pressure has to be 345 MPa (Fig. 2). Notably, the pressure corrections obtained at 500 and 300 MPa using the standard 19 mm assembly are in agreement with this trend, being +20 and +45 MPa, respectively. Combining all data in the pressure range 150–500 MPa, we obtain the expression for the pressure correction (Eq. (1), Fig. 3a). This correction has to be applied to the nominal pressure in order to obtain the equivalent real pressure on the sample:

$$P_{\text{correction}} (\text{MPa}) = -0.115 \times P_{\text{nominal}} (\text{MPa}) + 78.23 \quad (1)$$

Thus, the real pressure is expressed as follows (Fig. 3b):

$$P_{\text{real}} (\text{MPa}) = 1.13 \times P_{\text{nominal}} (\text{MPa}) - 87.56 \quad (2)$$

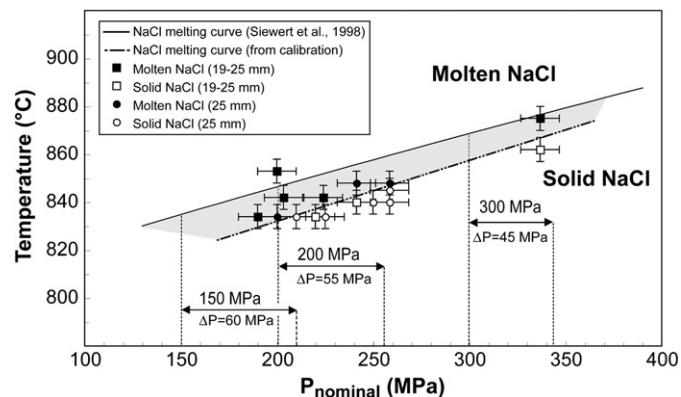


Fig. 2. Results of the NaCl calibration experiments performed using the 19–25 mm and 25 mm assemblies. The solid line is the NaCl melting curve (Siewert et al., 1998), the dotted line is the melting curve resulting from our NaCl calibration experiments and is obtained by visual interpolation. The shifting between the two lines, indicated by the arrows, represents the pressure correction.

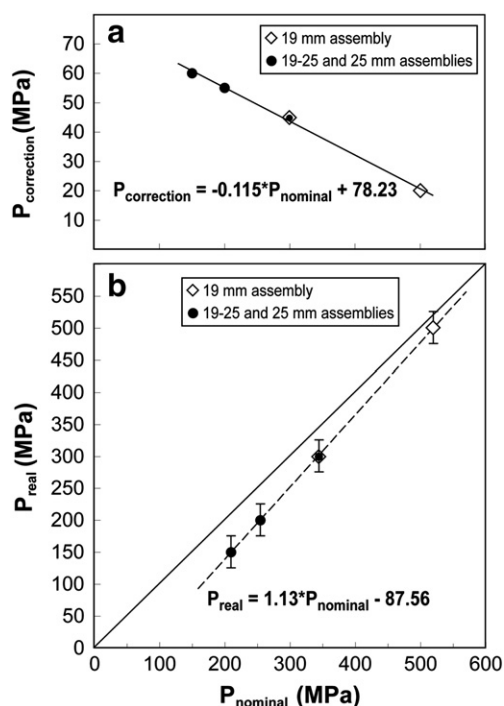


Fig. 3. (a) Pressure correction vs. nominal pressure diagram. Symbols denote pressure corrections in the pressure range 150–500 MPa, determined by means of the NaCl calibration experiments (see Fig. 2). The linear regression of the points yields the correction that has to be applied to the nominal pressure in order to have the equivalent real pressure on the sample. (b) Real pressure vs. nominal pressure diagram. The linear regression of the points yields the real pressure on the sample corresponding to the nominal pressure (force applied on the piston).

3.2. H₂O solubility experiments

The H₂O solubility experiments were performed in the 25 mm assembly using as starting materials the albitic glass used in Baker (2004) and an obsidian from Pietre Cotte lava flow (Vulcano Island, Southern Italy). Experimental data of Behrens et al. (2001) and the H₂O solubility model of Moore et al. (1998) provide reference models for H₂O solubility in albitic and rhyolitic melts, respectively.

Two capsules, loaded with albitic, glassy powder and either 4 wt.% or 10 wt.% deionised water (i.e. H₂O-undersaturated and H₂O-saturated conditions, respectively), were run in tandem for 2 h, at 900 °C, and at the real pressure of 200 MPa (see Eq. (2)). Three capsules, loaded with rhyolitic, glassy powder and 3.5, 7.5, and 11.8 wt.% deionised water were run for 24 h, at 975 °C and 150 MPa. In particular, capsules loaded with 3.5 and 11.8 wt.% deionised water (i.e. H₂O-undersaturated and H₂O-saturated conditions, respectively) were run in tandem. The weight of the capsule was checked before and after each experiment. Weight loss after piercing and drying at 110 °C the capsule revealed the presence of free water in the H₂O-saturated experiments. Moreover, images obtained by FE-SEM reveal the presence of bubbles, homogeneous in size and distribution, in glasses synthesized under H₂O-saturated conditions, whereas glasses synthesized in anhydrous and H₂O-undersaturated experiments are bubble-free (Fig. 4).

Chemical composition of hydrous glasses was compared with the composition of the nominally anhydrous glasses obtained by melting the starting materials at 1200 °C and ambient pressure in AuPd capsule (Table 2). Because all glasses (anhydrous, H₂O-undersaturated, and H₂O-saturated) are chemically homogeneous and comparable when normalized to 100 wt.% (Table 2), we can indirectly assess the pressure knowing the water concentration in glasses synthesized under H₂O-saturated conditions.

Dissolved H₂O in glasses was estimated using the “EPMA method”, assuming that the discrepancy between the analytical sum of the

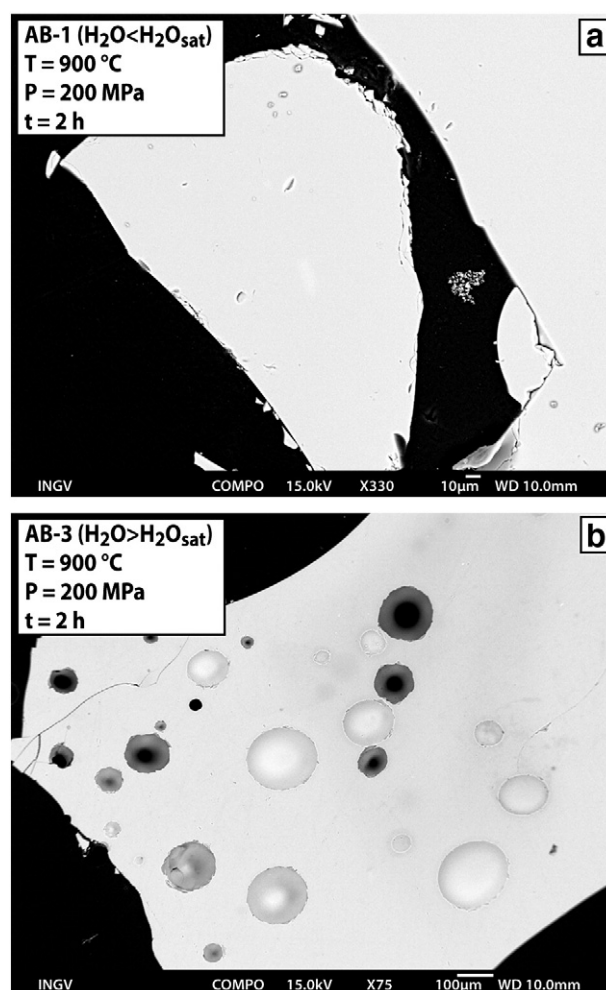


Fig. 4. FE-SEM images of H₂O-solubility experiments: (a) albitic bubble-free glass synthesized at H₂O-undersaturated conditions and (b) albitic bubble-bearing glass obtained under H₂O-saturated conditions.

microprobe analysis and 100 wt.% represents the H₂O concentration (Devine et al., 1995). Accordingly, the albitic glass synthesized under H₂O-saturated conditions contains 7.11 wt.% H₂O, which is ca. 0.6 wt.% higher than the 6.5 wt.% reported in Behrens et al. (2001). However, considering that analyses of anhydrous and H₂O-undersaturated glasses have the same 0.6 wt.% discrepancy from the expected total (e.g. 100 wt.% for the anhydrous and 96 wt.% for the H₂O-undersaturated run), we can reasonably assume that this difference is related to the analytical uncertainty rather than to an underestimate of the real pressure. The two rhyolitic glasses synthesized under H₂O-saturated conditions show H₂O contents of 4.8 and 5.5 wt.%. At the experimental conditions the solubility of water in the rhyolitic melt is about 5 wt.% (Moore et al., 1998), hence, in both cases, the difference between measured and predicted water concentration is within the 0.5 wt.% uncertainty of water estimate using the “EPMA method” (Devine et al., 1995). Note that the H₂O concentration in the H₂O-undersaturated glass is comparable with the initial weight of water in the charge.

It is worth noting that the above determined water contents in H₂O-saturated glasses lead to pressure estimates within the 25 MPa error associated to the NaCl calibration technique (Baker, 2004).

3.3. Comparison of calibration methods

Our calibration throughout NaCl melting curves demonstrates that the pressure correction decreases at a rate of approximately 1 MPa for

Table 2
Average composition of experimental glasses determined by EMPA, normalized to 100 wt.%.

Sample	AB-0		AB-1		AB-3		RIO-0		RIO-C6		RIO-C7		RIO-2	
T (°C)	1200		900		900		1200		975		975		975	
P (MPa)	0.1		205 ^a		205 ^a		0.1		150 ^a		146 ^a		146 ^a	
		sd(8)		sd(5)		sd(5)		sd(6)		sd(10)		sd(10)		sd(10)
SiO ₂	69.97	0.32	69.82	0.27	69.52	0.20	74.90	0.17	74.57	0.66	74.97	0.61	74.49	0.47
TiO ₂	–	–	–	–	–	–	0.11	0.04	0.07	0.06	0.15	0.04	0.12	0.06
Al ₂ O ₃	18.51	0.19	18.67	0.24	18.90	0.05	12.66	0.19	12.86	0.37	12.74	0.23	12.46	0.21
FeO _{tot}	–	–	–	–	–	–	1.72 ^b	0.17	1.70	0.09	1.48	0.17	1.76	0.13
MnO	–	–	–	–	–	–	0.10	0.02	0.05	0.03	0.08	0.05	0.08	0.04
MgO	–	–	–	–	–	–	0.11	0.04	0.16	0.03	0.11	0.04	0.18	0.04
CaO	–	–	–	–	–	–	0.81	0.06	0.97	0.08	0.90	0.05	0.91	0.07
Na ₂ O	11.49	0.18	11.47	0.25	11.51	0.13	4.09	0.16	4.10	0.05	4.16	0.13	4.35	0.21
K ₂ O	0.03	0.02	0.04	0.03	0.07	0.01	5.34	0.05	5.24	0.11	5.18	0.09	5.32	0.09
P ₂ O ₅	–	–	–	–	–	–	0.03	0.03	0.03	0.03	0.05	0.02	0.05	0.05
Cl	–	–	–	–	–	–	0.12	0.04	0.24	0.04	0.18	0.03	0.27	0.04
Total	100.00		100.00		100.00		100.00		100.00		100.00		100.00	
EMPA total	99.38 ^c		95.27		92.89		99.44 ^c		94.47		95.23		96.11	
H ₂ O (wt.%) ^d	0.0		4.0 (–)		10.0 (+)		0.0		7.5 (+)		11.8 (+)		3.5 (–)	
H ₂ O _{sol} (wt.%) ^e	–		6.50		6.50		–		5.02		4.92		4.92	
H ₂ O _{diff} (wt.%) ^f	–		4.73		7.11		–		5.53		4.77		3.89	

^a Real pressure (i.e. sample pressure), calculated from Eq. (2).

^b Recalculated as Fe₂O₃.

^c Discrepancy to 100 wt.% total of the nominally anhydrous samples AB-0 and RIO-0 can be explained as due to the EMPA analytical uncertainty.

^d Initial H₂O in the charges, (+) and (–) refer respectively to H₂O concentrations above and below theoretical H₂O saturation.

^e H₂O solubility in albitic and rhyolitic melt at the experimental conditions (see text for details).

^f H₂O determined using the “EPMA method” (100 – EPMA total).

every 10 MPa of increase in nominal pressure, over the investigated pressure range (Fig. 3). Both, 19–25 mm and 25 mm assemblies require the same pressure correction in the range 150–200 MPa. Notably, at 300 MPa the pressure correction for the new assemblies is the same as that found for the standard 19 mm assembly (Fig. 3), indicating that different sizes of the assembly components do not affect the pressure correction.

The uncertainty of the NaCl calibration method is associated with thermocouple accuracy (± 5 °C), yielding an error of ± 25 MPa for pressure determinations (Baker, 2004). This is comparable to the calibration based on the H₂O solubility in rhyolitic or albitic melt if the H₂O concentration is determined using the “EPMA method”. This error could be reduced by more accurate determination of dissolved water, through e.g., Fourier Transform Infra-Red spectroscopy or Karl-Fischer titration (cfr. Behrens et al., 1996). However, the comparison of the two calibration methods presented here is a rapid and inexpensive way to calibrate the piston cylinder. Our experiments demonstrate that the H₂O solubility calibration agrees with the NaCl calibration within the limits of the methods (i.e. in the range of 25 MPa). The main limitation of the NaCl calibration, if compared to the H₂O solubility method, is the very narrow NaCl melting temperature range (i.e. 830–870 °C in the pressure range 150–300 MPa). On the contrary, H₂O solubility experiments can be performed over a wide range of temperatures permitting the calibration at both low pressure and high temperature (e.g. P < 300 MPa, T > 900 °C). However, in this study, the pressure correction determined by the low temperature (830–870 °C) NaCl calibration experiments was confirmed by the high temperature (900–975 °C) H₂O solubility experiments. This result indicates that the NaCl method alone can be effectively used in low pressure calibrations for a wide range of temperatures (800–1000 °C). This method is the easier way to calibrate pressure in the piston cylinder (it does not require access to microprobe or FTIR), although it may require more experiments than the H₂O solubility method. Solubility experiments can be however employed to either verify the NaCl calibration over a range of different temperatures or as a monitor of pressure in multiple charge experiments.

4. Conclusions

This work demonstrates that using the proper assembly, here introduced as the 19–25 and 25 mm furnace assemblies, the piston cylinder apparatus can successfully perform experiments at pressure as low as 150 MPa. The large surface area of the assemblies implies a nominal pressure on the piston that is higher than that used for the standard 19 mm assembly. This makes the 19–25 and 25 mm assemblies more suitable for operating at pressure below 400 MPa, a value that represents the critical threshold for experiments performed with the standard 19 mm assembly. However, under low pressure conditions (i.e. 150 to 300 MPa), a progressively higher friction occurs and the nominal pressure needs to be increased at a rate of 1 MPa every 10 MPa.

Acknowledgements

We are grateful to D.R. Baker for illuminating the way towards “low pressure” possibilities, for useful discussion on instrumentation and calibration methods, and for providing the albitic glass. We are also grateful to the anonymous reviewer for his constructive review. A. Cavallo is thanked for his help during EMPA. This work is part of MM’s PhD programme and was funded by Sapienza – Università di Roma, Istituto Nazionale di Geofisica e Vulcanologia, Depths of the Earth Company, NSF EAR-0838563 to G. Moore, and Science Foundation Sweden to V.R. Troll.

References

- Baker, D.R., 2004. Piston-cylinder calibration at 400–500 MPa: a comparison of using water solubility in albite melt and NaCl melting. *American Mineralogist* 89, 1553–1556.
- Behrens, H., Romano, C., Nowak, M., Holtz, F., Dingwell, D.B., 1996. Near-infrared spectroscopic determination of water species in glasses of the system MAISI₃O₈ (M = Li, Na, K): an interlaboratory study. *Chemical Geology* 128, 41–63.
- Behrens, H., Meyer, M., Holtz, F., Benne, D., Nowak, M., 2001. The effect of alkali ionic radius, temperature, and pressure on the solubility of water in MAISI₃O₈ melts (M = Li, Na, K, Rb). *Chemical Geology* 174, 275–289.

- Bohlen, S.R., 1984. Equilibria for precise pressure calibration and a frictionless furnace assembly for the piston-cylinder apparatus. *Neues Jahrbuch für Mineralogie, Monatshefte* 9, 404–412.
- Boyd, J.R., England, J.L., 1960. Apparatus for phase-equilibrium measurements at pressures up to 50 kilobars and temperatures up to 1750 °C. *Journal of Geophysical Research* 65, 741–748.
- Devine, J.D., Gardner, J.E., Brack, H.P., Layne, G.D., Rutherford, M.J., 1995. Comparison of microanalytical methods for estimating H₂O contents of silicic volcanic glasses. *American Mineralogist* 80, 319–328.
- Freda, C., Baker, D.R., Ottolini, L., 2001. reduction of water loss from gold–palladium capsules during piston-cylinder experiments by use of pyrophyllite powder. *American Mineralogist* 86, 234–237.
- Freda, C., Gaeta, M., Misiti, V., Mollo, S., Dolfi, D., Scarlato, P., 2008. Magma–carbonate interaction: an experimental study on ultrapotassic rocks from Alban Hills (Central Italy). *Lithos* 101, 397–415.
- Holloway, J.R., Wood, B.J., 1988. *Simulating the Earth*. Unwin Hyman, Winchester, Massachusetts. 196 pp.
- Holtz, F., Becker, A., Freise, M., Johannes, W., 2001. The water-undersaturated and dry Qz-Ab-Or system revisited. Experimental results at very low water activities and geological implications. *Contributions to Mineralogy and Petrology* 141, 347–357.
- Johannes, W., Bell, P.M., Mao, H.K., Boettcher, A.I., Chipman, D.W., Hays, J.F., Newton, R.C., Seifert, F., 1971. An interlaboratory comparison of piston-cylinder pressure calibration using the albite-breakdown reaction. *Contributions to Mineralogy and Petrology* 32, 24–38.
- Masotta, M., Freda, C., Gaeta, M., 2012. Origin of crystal-poor, differentiated magmas: insights from thermal gradient experiments. *Contributions to Mineralogy and Petrology* 163, 49–65.
- Moore, G., Vennemann, T., Carmichael, I.S.E., 1998. An empirical model for the solubility of H₂O in magmas to 3 kbar. *American Mineralogist* 83, 36–42.
- Moore, G., Roggensack, K., Klonowski, S., 2008. A low-pressure-high-temperature technique for the piston-cylinder. *American Mineralogist* 93, 48–52.
- Nelson, S.T., Montana, A., 1992. Sieve-textured plagioclase in volcanic rocks produced by rapid decompression. *American Mineralogist* 77, 1242–1249.
- Siewert, R., Büttner, H., Rosenhauer, M., 1998. Experimental investigation of thermodynamic melting properties in the system NaCl–KCl at pressures of up to 7000 bar. *Neues Jahrbuch für Mineralogie, Abhandlungen* 172, 259–278.